Existence of isostatic, maximally random jammed monodisperse hard-disk packings

Steven Atkinson[a], Frank H. Stillinger[b,1], and Salvatore Torquato[b,c]

[a]Department of Mechanical and Aerospace Engineering, [b]Department of Chemistry, and [c]Department of Physics, Princeton University, Princeton, NJ 08544

Edited by Morrel H. Cohen, Rutgers, The State University of New Jersey, Bridgewater Township, NJ, and approved November 18, 2014 (received for review May 7, 2014)

We generate jammed packings of monodisperse circular hard-disks in two dimensions using the Torquato–Jiao sequential linear programming algorithm. The packings display a wide diversity of packing fractions, average coordination numbers, and order as measured by standard scalar order metrics. This geometric-structure approach enables us to show the existence of relatively large maximally random jammed (MRJ) packings with exactly isostatic jammed backbones and a packing fraction (including rattlers) of $\phi = 0.826$. By contrast, the concept of random close packing (RCP) that identifies the most probable packings as the most disordered misleadingly identifies highly ordered disk packings as RCP in 2D. Fundamental structural descriptors such as the pair correlation function, structure factor, and Voronoi statistics show a strong contrast between the MRJ state and the typical hyperstatic, polycrystalline packings with $\phi \approx 0.88$ that are more commonly obtained using standard packing protocols. Establishing that the MRJ state for monodisperse hard disks is isostatic and qualitatively distinct from commonly observed polycrystalline packings contradicts conventional wisdom that such a disordered, isostatic packing does not exist due to a lack of geometrical frustration and sheds light on the nature of disorder. This prompts the question of whether an algorithm may be designed that is strongly biased toward generating the monodisperse disk MRJ state.

packing | jamming | randomness

A packing in d-dimensional Euclidean space $\mathbb{R}^d$ is defined as a collection of particles that do not overlap with one another. In three dimensions (3D), hard particle packings have served as simple, yet powerful models for a wide variety of condensed matter systems including liquids, glasses, colloids, particulate composites, and biological systems, to name a few (1–5). In two dimensions (2D), they have been used to model systems such as the molecular structure of monolayer films (6, 7), adsorption of molecules on substrates (8, 9), and the organization of epithelial cells (10, 11). Moreover, particular interest has been devoted toward packings that are jammed (roughly speaking, packings that are mechanically stable) (12–18).

Jammed packings of monodisperse spheres in 3D exist over a wide range of packing fractions from $\phi = \pi/\sqrt{18} \approx 0.74048\ldots$ to $\phi = \pi\sqrt{2}/9 \approx 0.49365\ldots$, where the former corresponds to the fcc lattice, and the latter corresponds to the "tunneled crystals" (19). In addition, jammed packings exist with intermediate packing fractions and a wide variety of order, including packings that are fully noncrystalline. Of particular interest is the "maximally random jammed" (MRJ) state, defined as the packing that minimizes some scalar order metric ψ subject to the jamming constraint, replacing the familiar notion of random close packing (RCP) (20), originally defined as the densest configuration that a "random" packing could attain without ever defining "randomness." The concept of the MRJ state is a natural outcome of the geometric-structure approach, in which packings are analyzed primarily on an individual basis.

The situation for disordered monodisperse disk packings in 2D is very different from the 3D counterpart because the former lacks geometrical frustration, i.e., the densest local packing arrangement is compatible with the globally densest packing arrangement (the triangular lattice). As a result, packing protocols have struggled to generate disordered, jammed packings of monodisperse disks, suggesting that the most disordered packing is a polycrystalline arrangement—a dubious proposition for the MRJ state. Nonetheless, a truly disordered, jammed disk packing has remained elusive. Here we show by construction, using the geometric-structure approach, that the MRJ state for monodisperse disks is not polycrystalline; rather, it is isostatic and significantly more disordered as measured by bond-orientational and translational order metrics, as well as its vivid visual impression.

To formalize the concept of jamming, Torquato and Stillinger have provided rigorous definitions for local, collective, and strict jamming (12). Because collectively jammed packings are stable to uniform compression, and strictly jammed packings are additionally stable against shear deformations, we will restrict ourselves to considering only these two categories of jamming for the purposes of our current work. It is not uncommon to find that some subset of particles is jammed (the backbone) while the remainder are not jammed but are locally imprisoned by their neighbors (the rattlers). If there is no jammed backbone, then the packing is unjammed. Note that, unless specified otherwise, packings are typically characterized (e.g., in order maps) while including rattlers.

The family of jammed packings is conveniently described via "order maps" that classify packings according to their packing fraction, order metric, and whether or not they are jammed. Fig. 1 provides a schematic order map for 3D frictionless monodisperse sphere packings. We first contrast a schematic order map for the 2D case in Fig. 2 that has some important distinctions. In 3D, the densest packing is the fcc lattice or its stacking variants (line B–B' in Fig. 1). By contrast, in 2D, the densest packing, the triangular lattice, is unique; therefore, it is

Significance

Disordered particle packings are ubiquitous in all areas of science. Although disordered jammed packings of hard spheres are readily observed in 3D, the story is quite different for disks. Most 2D packing protocols tend to produce highly ordered disk arrangements, suggesting that truly disordered jammed disk packings might not exist in 2D. The maximally random jammed (MRJ) configurations we observe have a complete lack of crystallinity and are distinct from the typical jammed configuration that is most probable upon rapid compression. A protocol-independent geometric-structure approach allows us to create, identify, and analyze these previously elusive packings. Our results shed new light on the nature of randomness, which is an issue that arises across the physical, mathematical, and biological sciences.

Author contributions: S.T. designed research; S.A., F.H.S., and S.T. performed research; S.A., F.H.S., and S.T. contributed new reagents/analytic tools; S.A., F.H.S., and S.T. analyzed data; and S.A., F.H.S., and S.T. wrote the paper.

The authors declare no conflict of interest.

This article is a PNAS Direct Submission.

[1]To whom correspondence should be addressed. Email: fhs@princeton.edu.

This article contains supporting information online at www.pnas.org/lookup/suppl/doi:10.1073/pnas.1408371112/-/DCSupplemental.

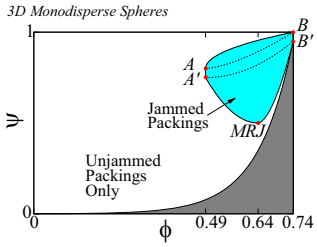


Fig. 1. Schematic order map in the density–order (ϕ–ψ) plane for 3D strictly jammed, frictionless, monodisperse hard-sphere packings, adapted from ref. 16. White and blue regions contain the attainable packings, the blue region represents the jammed subset of packings, and the dark shaded region contains no packings. The locus of points *A*–*A*′ corresponds to the lowest-density jammed packings, conjectured to be tunneled crystals with $\phi = \pi\sqrt{2}/9$ (19). The locus of points *B*–*B*′ corresponds to the densest jammed packings (stacking variants of the fcc lattice). Packings along the curves joining these extrema can be generated by randomly inserting spheres into the vacancies of the tunneled crystal until the corresponding fcc variant is obtained. The point MRJ represents the maximally random jammed state, i.e., the most disordered state subject to the jamming constraint.

represented by a single point *B* in Fig. 2. In a similar manner, the least dense jammed 3D sphere packing, conjectured to be the tunneled crystal (19), is not unique, and has stacking variants; these populate the line *A*–*A*′ in Fig. 1. Similarly in 2D, the analogous reinforced kagomé lattice packings [conjectured to be the least dense jammed disk packings (21)] populate the line *A*–*A*′ in Fig. 2, and are generated by altering the way in which vacancies are selected from the triangular lattice. In both 2D and 3D, intermediate packings may be generated by filling in the vacancies in these packings (curves *A*–*B* and *A*′–*B*′ in 3D, and *A*–*B* and *A*′–*B* in 2D).

It is important to note that the order map paradigm is protocol-independent and does not conflate existence with frequency of observation. Just as the reinforced kagomé lattice is an interesting structure that is elusive to typical packing protocols, the MRJ state is interesting in its own right, regardless of how (often) it is observed. A characterization of the MRJ state by construction is thus of general interest.

Similarly, the MRJ state is protocol-independent and quantifies the order of an individual packing, regardless of its frequency of occurrence, i.e., using a geometric-structure approach (16). This is to be contrasted to the current prevailing definition of RCP, in which an entropic measure is used to define randomness, i.e., that

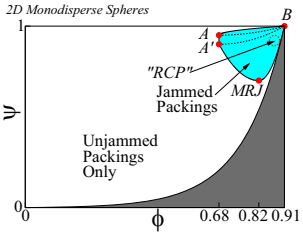


Fig. 2. Schematic order map in the density–order (ϕ–ψ) plane for 2D strictly jammed, frictionless, monodisperse hard-disk packings in the infinite-system limit. White, blue, and dark-shaded regions are the same as in Fig. 1. The locus of points *A*–*A*′ corresponds to the lowest-density jammed packings, conjectured to be the reinforced kagomé lattice, reinforced rectangular kagomé lattice, and other combinations, all with $\phi = \pi\sqrt{3}/8$ (12). The point *B* corresponds to the triangular lattice. Packings along the curves joining these extrema can be generated by randomly inserting spheres into the vacancies of the packings found along *A*–*A*′ lattice until the triangular lattice is obtained. The point *MRJ* represents the maximally random jammed state. The entropically defined location of RCP is labeled to stress the difference between using ensemble-based and geometric-structure approaches.

RCP packings are an ensemble of jammed configurations that are the most probable outcome upon uniformly densifying a random initial configuration to the point of jamming (13–15, 22, 23). Such an ensemble-based definition implies that the most probable configurations represent the most disordered state. This is a reasonable postulate because entropy is the standard way of thinking about randomness in thermodynamic systems, and indeed the distinction is subtle for spheres in 3D because the packing fraction of the MRJ state seems to be coincident with such a location in phase space based on information gathered from many standard protocols (13, 20, 24–27). However, many other properties, such as the degree of order (as measured by the standard scalar order metrics) and rattler attributes have been found to vary in disordered packings at the MRJ packing fraction depending upon the protocol used to generate them. In other words, packing fraction alone is not sufficient to characterize a disordered jammed packing (27–29).

The distinction between the geometric-structure and ensemble-based approaches is even more critical in 2D, especially for monodisperse disk packings. In particular, the lack of "frustration" (30, 31) in 2D analogs of 3D computational and experimental protocols that lead to putative RCP states result in highly crystalline packings, forming rather large triangular coordination domains (grains) (21, 26, 32). Because such highly ordered packings are the most probable outcomes for these typical protocols, "entropic measures" of disorder misleadingly identify these as the most disordered. This has even caused some to hypothesize that RCP does not exist at all for monodisperse disks (33). An appropriate order metric, on the other hand, is capable of identifying a particular configuration (not an ensemble of configurations) that is consistent with one's intuitive notion of maximal disorder. However, typical packing protocols do not generate such large disordered disk configurations due to their inherent implicit bias toward undiluted crystallization. It has been suggested that jammed packings with a significantly lower ϕ and ψ exist (16, 34); the geometric-structure approach involved in the definition of the MRJ state is necessary to identify such packings, even if rare with respect to most protocols, as highly disordered.

Before the advent of these aforementioned rigorous definitions of jamming and the MRJ state, numerous attempts were made to generate RCP packings of monodisperse disks (6, 25, 35–38). Upon devising a rigorous jamming test (39), these results were revisited, and it was found that these packings were not even collectively jammed (21).

The Torquato–Jiao (TJ) linear programming algorithm (40) can be used to generate sphere packings in an arbitrary dimension that are guaranteed a priori to be strictly jammed. In addition, the sphere packings that it produces in $d \geq 3$ are exactly isostatic with high probability. [An isostatic packing is one that is jammed and has the minimum number of contacts required for mechanical stability. In 2D, this is $z = 4 - 2/N_B$ for collective jamming and $z = 4 + 2/N_B$ for strict jamming, where N_B is the number of backbone disks (41).] It has been used recently to provide new details to the nature of the MRJ state in 3D (27).

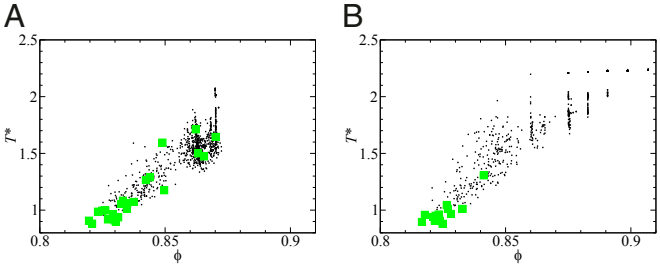


Fig. 3. Order maps of disk packings that are (*A*) collectively jammed and (*B*) strictly jammed. Initial configurations were generated from RSA with $\phi_{init} = 0.10$. Isostatic packings are shown as green squares.

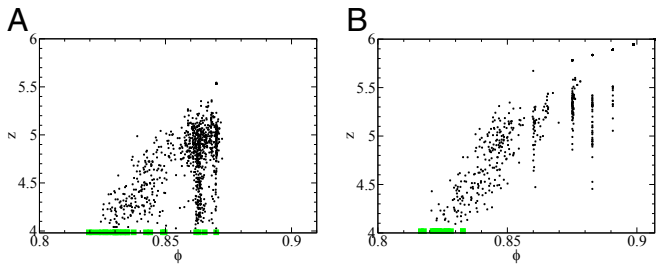


Fig. 4. The ϕ–*z* projection of the three-axis order map for 1,000 (*A*) collectively jammed and (*B*) strictly jammed packings generated from RSA with $\phi_{init} = 0.10$. Isostatic packings are shown as green squares.

Given its promising abilities in generating disordered, jammed sphere packings in 3D, we now turn our attention toward the 2D problem to see if it might provide new insights.

We use the TJ algorithm to produce collectively and strictly jammed packings of monodisperse disks that are exactly isostatic and lack any sixfold-coordinated disks. These packings are characterized according to their packing fraction and order using bond-orientational and translational order metrics to determine the candidates for the MRJ state. We also present pair correlation function and Voronoi statistics. The packings that we have generated demonstrate the existence of an isostatic MRJ state in 2D that is fundamentally different from the polycrystalline packings produced by typical protocols.

Packing Generation

Here, we use the TJ algorithm to generate frictionless jammed packings of monodisperse disks within a fundamental cell (FC) with periodic boundary conditions. The process may be broken into two steps: generating initial configurations and densifying said configurations to the point of jamming.

Because TJ is very sensitive to the initial configuration, we explored a variety of initial configurations. The first of these was the usual random sequential addition (RSA), carried out at a low packing fraction (typically 0.10) so as to approximate a Poisson process. We also explored several FC shapes including the usual square FC as well as slightly distorted FCs to aid in causing geometric frustration. We also tried a rhombic FC with interior angle $\pi/3$, which is compatible with the triangular lattice if the number of disks is a square integer.

To explore disordered packings at higher initial packing fractions, we used the serial algorithm for generating packings with controlled orientational order introduced in ref. 42 and the version in which no orientational preference is indicated [i.e., the Eden model (43) adapted to hard disks].

The final initial condition ensemble that we considered was created by generating bidisperse disk packings with number ratio 0.5 and diameter ratio 1.4. Initial conditions for the bidisperse packing were generated via RSA at low packing fraction; the packing was subsequently jammed using TJ. The large disks in the resulting jammed configurations were then shrunk so that the packings became monodisperse; these packings were then fed back to TJ to yield jammed monodisperse disk packings.

The TJ algorithm (40) uses an iterative process to densify packings of hard spheres in an arbitrary dimension using a linear optimization scheme to maximize ϕ to first order by shrinking the FC. The optimization variables are the N displacement vectors for the spheres in the system (Nd variables) as well as the symmetric strain tensor that deforms and shrinks the FC ($d(d+1)/2$ variables). The constraints are that no pair of spheres may overlap (to a locally linear approximation). By iteratively solving this linear program (LP), one obtains a local packing fraction maximum of the initial configuration. Furthermore, when the LP cannot find any further densification up to some numerical threshold, the packing is guaranteed to be strictly jammed to a corresponding tolerance, and is therefore a local packing fraction maximum. Furthermore, if the FC is disallowed from deforming (i.e., its shape is preserved), the packing is instead guaranteed to be collectively jammed. For mathematical details, see the *Materials and Methods*.

Results

We generated at least 10^4 packings per system size ($10 \le N \le 200$) per initial condition for both collective and strict jamming. The following subsections characterize various statistical and geometrical details of the packings.

Order Maps. We begin by presenting order maps of the packings that we have generated. Fig. 3 *A* and *B* show scatter plots of collectively and strictly jammed packings, respectively. The packings were generated with (Fig. 3*A*) $N = 150$ and (Fig. 3*B*) $N = 110$ from RSA initial conditions in a rhombic FC with interior angle $2\pi/5$. Isostatic packings are shown as green squares. The order metric ψ used here is the pair correlation function-based order metric T^* (44), defined as

$$T^* = \frac{\int_{D\rho^{1/d}}^{\xi_c} |g_2(\xi) - 1| d\xi}{\xi_c - D\rho^{1/d}},$$

where D is the disk diameter, $\xi = r\rho^{1/d}$ is a dimensionless distance, $g_2(\xi)$ is the isotropic pair correlation function, $\rho = N/V$ is the number density, and ξ_c is a dimensionless cutoff value, chosen here to be 3. For most monodisperse disk packings, this corresponds to a pair distance that is slightly less than three diameters. The quantity T^* may be thought of as a "disorder metric" in that it quantifies the amount by which a packing differs from a Poisson point process, for which $g_2 = 1$ everywhere. It is interesting to note that the MRJ state for monodisperse disks is nearly as disordered (as quantified by T^*) as typical disordered packings of bidisperse disks with diameter ratio between unity and 1/1.4, which more readily exhibit disordered, isostatic jammed states; see the *SI Appendix* for further details. One may also consider other order metrics aside from T^*; we discuss this as well in the *SI Appendix*.

We expand the traditional order map paradigm here by adding a third axis: the average backbone coordination number, z (16). Projections of this three-axis (ϕ–ψ–z) order map onto the ϕ–z and ψ–z planes are shown in Figs. 4 and 5, respectively; again, we chose to use T^* as our order metric. This expanded picture shows that, as the degree of order decreases and the MRJ state is approached, the range of z narrows toward isostaticity, implying that the MRJ state for monodisperse disks has an isostatic backbone, just as is the case for MRJ packings of hard spheres in 3D (27).

For collective jamming, the MRJ state has a packing fraction of 0.826 ± 0.001 and a rattler fraction of $N_R/N = 0.035 \pm 0.002$; for strict jamming these values are $\phi = 0.826 \pm 0.002$ and

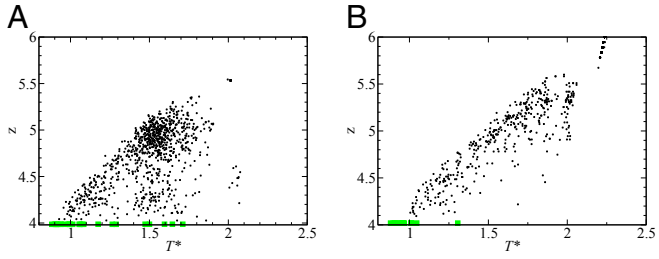


Fig. 5. The ψ–*z* projection of the three-axis order map for 1,000 (*A*) collectively jammed and (*B*) strictly jammed packings generated from RSA with $\phi_{init} = 0.10$; the order metric used here is the g_2-based order metric T^*. Isostatic packings are shown as green squares. As T^* decreases, the distribution of packings in terms of coordination number narrows toward isostaticity.

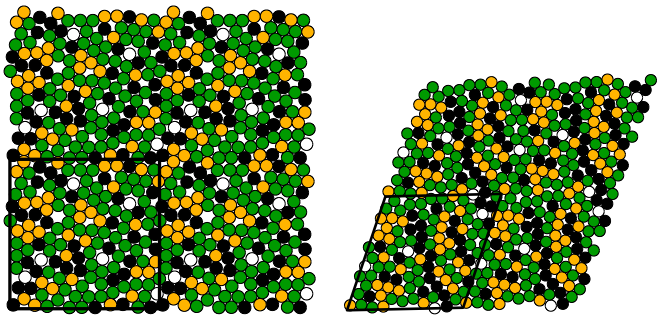


Fig. 6. Examples of exactly isostatic, (*Left*) collectively jammed and (*Right*) strictly jammed monodisperse disk packings with $N = 150$ and 110 disks, respectively. Disks are colored to indicate their (backbone) coordination as follows: dark blue = 3 contacts, green = 4 contacts, orange = 5 contacts, and white = rattler (0 contacts). The fundamental cell is outlined in black.

$N_R/N = 0.034 \pm 0.004$. The rattler fraction is significantly higher than that for the MRJ state for 3D (27) and obeys the general trend that the rattler fraction tends to decrease as d increases (45). We reiterate that our packings are fundamentally different from previously obtained disordered disk packings in that our packings are collectively or strictly jammed, whereas previous attempts failed to produce packings that were even collectively jammed (and, in some cases, locally jammed; a locally jammed packing is one in which no particle may be moved while holding all other particles fixed. This jamming category is insufficient to guarantee mechanical stability of any sort.). Thus, we are demonstrating the existence of mechanically stable packings that are significantly disordered when compared to the usual polycrystalline packings generated by most protocols. It is important to note that these packings demonstrate an isostatic MRJ state for 2D that is distinct from the polycrystalline state that standard jamming protocols tend to produce. Examples of isostatic MRJ packings are given in Fig. 6.

Several isostatic, collectively jammed packings were found with relatively high ϕ and ψ (see Fig. 3*A*), which to our knowledge are also outcomes unique to the TJ algorithm. Closer inspection reveals that these packings possess large distorted grains similar to those observed in ref. 26. This can be explained by noting that the FC shape was incompatible with the triangular lattice, introducing frustration into near-crystalline domains. Allowing the cell to deform (as is done for strict jamming) eliminates these isostatic high-ϕ, high-ψ packings by allowing them to collapse into hyperstatic configurations.

Success Rate. Using TJ, we have found that the probability of producing a packing with an isostatic backbone decreases in a roughly exponential manner as N increases; although the choice of initial configuration and FC shape cannot be disregarded, in general, the probability for $N = 100$ is approximately 3×10^{-3} for collective jamming and 2×10^{-4} for strict jamming; this probability decreases by a factor of 10 for every 40 additional disks. Details are available in the *SI Appendix*. Although this exponential decay may be the case for the present algorithm, there is no apparent reason why isostatic, MRJ packings would not exist for arbitrarily large system sizes; it is of interest to devise a protocol that increases their frequency of occurrence.

Pair Correlation Function. We have produced 16 packings with $N = 150$ and 177 packings with $N = 100$ that are exactly isostatic and representative of the MRJ state for collective jamming; for strict jamming, we found 28 packings with $N = 110$. To contrast these packings with the typical results ("ensemble average") generated by the TJ protocol, we randomly selected 1,000 collectively jammed packings with $N = 150$ and 1,000 strictly jammed packings with $N = 110$.

Fig. 7 *A* and *B* shows the pair correlation function $g_2(r)$ for collectively and strictly jammed packings, respectively. The peaks that correspond to the triangular lattice geometry are considerably suppressed among the MRJ packings compared with the ensemble averages. This stresses the significant qualitative differences between the MRJ state and the most common states. The corresponding structure factors are given in the *SI Appendix*.

Hyperuniformity. We have found that number density fluctuations in our MRJ packings grow more slowly than the area of a (randomly placed) observation window, implying that the MRJ state is hyperuniform (infinite-wavelength density fluctuations vanish; ref. 46) in 2D (*SI Appendix*). This is to be contrasted with typical 2D disordered systems in which the variance grows in proportion to the window area. The 3D MRJ packings have also been shown to be hyperuniform with quasi-long-range order (47).

Voronoi Statistics. Voronoi diagrams were created using the point patterns of the disk centers. Fig. 8 shows the probability distribution of the number of sides per Voronoi cell for isostatic packings as well as for a full ensemble average. Although most cells are hexagons in both cases, it is clear that the isostatic packings exhibit a much larger variability. In addition, although most hexagons in polycrystalline packings are regular, corresponding to a locally close-packed configuration, this is far from the case for the isostatic packings. Distributions of the local packing density of the Voronoi cells are shown in the *SI Appendix*.

Discussion

We have used the TJ algorithm to produce collectively and strictly jammed packings of monodisperse disks that are exactly isostatic with system sizes up to $N = 150$ and 100, respectively. These isostatic packings are hyperuniform, have an average packing fraction of $\phi = 0.826$, and are significantly more disordered than the polycrystalline packings generated by typical protocols. In fact, these packings are candidates for the MRJ state according to bond-orientational and translational order metrics. The pair correlation function includes spikes corresponding to some of the local geometries found in the triangular lattice, but they are strongly suppressed in comparison with the ensemble average. In a similar manner, the presence of six-sided Voronoi cells corresponding to hexagonal close packing is strongly suppressed, and a variety of other geometries have arisen, including the increased presence of nonhexagonal Voronoi cells.

It is well known that the MRJ state for monodisperse spheres in 3D is isostatic. In addition, polydisperse disk packings in 2D have been a popular way to elicit disordered packings, which are often isostatic (13, 14, 17, 40). However, an isostatic packing of monodisperse disks has proved to be elusive until now. Although they remain difficult to obtain, we have shown that they do in fact exist, and that some of them have properties that are consistent with what one should expect from the MRJ state.

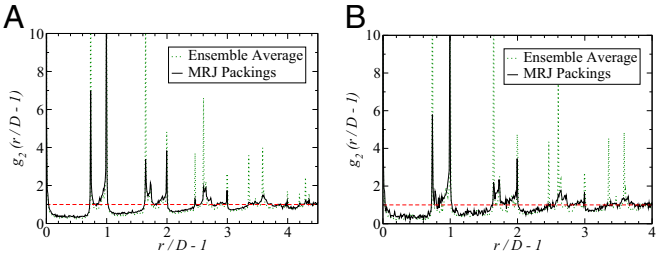


Fig. 7. Pair correlation function for exactly isostatic, MRJ packings (black solid lines) and the ensemble average (dotted green lines) for (*A*) collective and (*B*) strict jamming. Peaks that correspond to features of the triangular lattice that are usually found in polycrystalline packings are considerably suppressed in the MRJ state. A red dashed line showing $g_2 = 1$ is shown as a guide for the eye.

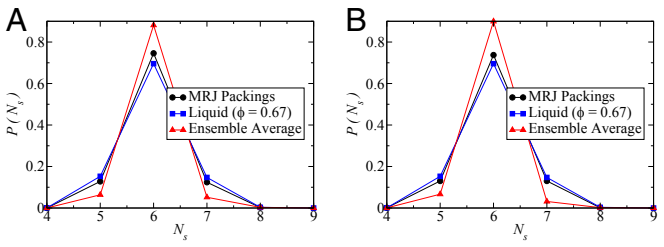


Fig. 8. Probability distribution for the number of edges per Voronoi cell for (*A*) collectively and (*B*) strictly jammed disk packings. In addition to the MRJ packings and the ensemble average, data for the equilibrium hard-disk fluid with packing fraction $\phi = 0.67$ is included for the sake of comparison.

It is critical to point out that the 2D MRJ packings that we have shown are not entropically favored. This is problematic for a picture of RCP that relies on one's choice of protocol as well as an ensemble-based, entropic definition. Assuming that one chooses an algorithm that is capable of producing disordered, isostatic packings, one still risks being misled by the likelihood that most packings will be highly ordered, hyperstatic polycrystalline packings, concluding that RCP is a rather unsatisfying concept in 2D. Rather, one must use a geometric-structure approach and apply some order metric that is well defined for any single packing. This method not only allows one to unambiguously identify disorder in packings without relying on a particular packing protocol, but is also able to identify disorder in a manner that is more consistent with one's intuition. Our findings in this work call into question the merits of studying RCP by means of an entropic, ensemble-based methodology because of the misleading picture it presents for 2D monodisperse disks.

In 3D, the least dense jammed packing known, the tunneled crystal, is hyperstatic: every sphere is sevenfold-coordinated, i.e., $z = 7$. By contrast, the reinforced kagomé (the least dense packing in 2D) lattice is isostatic in the infinite-system limit with average coordination number $z = 4$. What happens between these extremal points and the MRJ points in the jammed subsection of the order map? Although some transition from $z = 6$ to 7 is expected in 3D, it is unclear whether there is an isostatic continuum of packings connecting the MRJ state and reinforced kagomé lattice in 2D. One possible picture is that the triangular lattice and reinforced kagomé lattice both represent states with an infinitely large crystal; by reducing the grain size, disorder increases until the MRJ point is reached. Then, as the continuum from the MRJ point to the triangular lattice may be spanned by slowly growing crystalline grains within the packing, the continuum from MRJ to reinforced kagomé may be spanned by growing diluted crystals.

Demonstrating the MRJ state for monodisperse disks by construction is important conceptually in a similar way to the discovery of the reinforced kagomé lattice in that both are extremal packings that are very interesting although hard to observe via traditional packing protocols. This reflects a persisting fundamental lack of knowledge that we still have with regards to designing packing protocols; nevertheless, the MRJ state for disks is an interesting state because it represents an extreme state within the confines of the jamming constraint. This prompts an algorithmic question: can one devise a packing protocol that favors MRJ-like states for hard disks? Remarkable examples of biological processes that suppress crystallization have already been found in nature such as thermal hysteresis antifreeze proteins, found in both overwintering insects and polar marine fishes (48, 49), and may be used to inspire the design of specialized packing protocols and, in turn, materials synthesis techniques.

The question, "What is randomness?" is an extremely fundamental, ubiquitous question arising in not only physics and chemistry, but mathematics and biology as well. By uncovering the MRJ state for hard disks, we identify a serious challenge to the traditional notion of disorder—that the most probable distribution is correlated with randomness. We have shown here such a distribution that is not correlated with disorder at all; the most disordered jammed configuration is not the one that shows up the most frequently in any known protocol. On the other hand, we confirm that certain order metrics are capable of accurately characterizing the order of packings on an individual basis even in this challenging case. Moreover, these revelations concerning randomness are not limited to hard-particle packings: what does the MRJ state look like for real-world systems such as water molecules or polymers? The geometric-structure approach appears to provide the proper groundwork for considering such questions.

Materials and Methods

The densification process that the TJ algorithm performs is an iterative procedure driven by solving linear programs (LPs). The protocol goal is to maximize ϕ [or, in the energy landscape picture (40), minimize $-\phi$], and so we may pose an objective function in terms of a strain tensor ε acting on the fundamental cell's generating matrix Λ. A linearization gives the following objective function for the LP:

$$\min \mathrm{Tr}(\boldsymbol{\epsilon}) = \epsilon_{11} + \epsilon_{22} + \epsilon_{33} + \ldots + \epsilon_{dd}. \qquad [1]$$

This implies that the components of the strain tensor ε are design variables; the other variables are the displacements for each sphere (in the lattice coordinate system), $\Delta\boldsymbol{x}_1^\lambda, \Delta\boldsymbol{x}_2^\lambda, \Delta\boldsymbol{x}_3^\lambda, \ldots, \Delta\boldsymbol{x}_N^\lambda$, all of which are d-dimensional vectors, where lambda denotes that the vectors are expressed in terms of Λ. Because no two spheres can overlap, our LP's constraints must reflect that r_{mn}^G, the (global) distance between the centroids of spheres m and n; with diameters D_m and D_n, respectively; be $r_{mn}^g \geq 1/2(D_m + D_n)$. Expressing this in terms of the spheres' lattice coordinates, and taking into account the spheres' displacements and deformable fundamental cell, we have $\sqrt{\boldsymbol{r}_{mn}^\lambda \cdot \boldsymbol{\Lambda} \cdot (1+\epsilon)^2 \cdot \boldsymbol{\Lambda} \cdot \boldsymbol{r}_{mn}^\lambda} \geq (D_i + D_j)/2$, where the relative displacement $\boldsymbol{r}_{mn}^\lambda = (\boldsymbol{x}_n^\lambda + \Delta\boldsymbol{x}_n^\lambda) - (\boldsymbol{x}_m^\lambda + \Delta\boldsymbol{x}_m^\lambda)$. Linearizing this gives

$$\begin{aligned} \boldsymbol{\Lambda} \cdot \boldsymbol{r}_{nm}^\lambda \cdot \boldsymbol{\epsilon} \cdot \boldsymbol{\Lambda} \cdot \boldsymbol{r}_{nm}^\lambda + \Delta\boldsymbol{x}_m^\lambda \cdot \mathbf{G} \cdot \boldsymbol{r}_{nm}^\lambda + \Delta\boldsymbol{x}_n^\lambda \cdot \mathbf{G} \cdot \boldsymbol{r}_{mn}^\lambda \\ \geq \frac{1}{2}\left((D_m + D_n)/2 - \boldsymbol{r}_{nm}^\lambda \cdot \mathbf{G} \cdot \boldsymbol{r}_{nm}^\lambda\right) + \mathcal{R}, \end{aligned} \qquad [2]$$

where $\mathbf{G} = \boldsymbol{\Lambda}^T \cdot \boldsymbol{\Lambda}$ is the Gram matrix of the lattice Λ and $\mathcal{R}$ contains all of the higher-order terms; in practice, it is acceptable to let $\mathcal{R} = 0$. An influence sphere of radius γ is defined such that a constraint will be included in the LP for any pair of spheres whose centroids are separated by less than $(D_m + D_n)/2 + \gamma$. Because Eq. **2** is a local linearization of a quadratic constraint, we impose an artificial limit on the extent of the design variables in each iteration to preserve the accuracy of the linearization.

If we replace the strain tensor ε with a scalar, we constrain the shape of the fundamental cell to remain constant. In such a way, the TJ algorithm can be quickly modified to produce collectively jammed packings instead of strictly jammed packings. This LP is solved to determine how the packing will be rearranged and densified. After applying the sphere displacements and lattice deformation, the LP is reformulated using the new sphere positions and the fundamental cell's generating matrix. The process is iterated until the solution converges and the packing does not change by more than some termination threshold. We have found that the most effective threshold is the fundamental cell volume; when the cell volume fails to decrease by an appreciable amount, the packing is jammed to a corresponding precision.

Packings are compressed using the TJ algorithm with an influence sphere of diameter $\gamma = D/40$ (40), where D is the diameter of a sphere. For a single LP iteration, box deformations (both normal and shear movements) are limited in magnitude to less than $D/200$ and sphere translations are limited to $\|\Delta\boldsymbol{r}_i\| \leq D/200$. The algorithm is terminated when two successive compressions fail to decrease the lattice volume by $V_k - V_{k-2} < 2.0 \times 10^{-12}$, where V_k is the volume of the fundamental cell on iteration k.

ACKNOWLEDGMENTS. This work was supported in part by the National Science Foundation under Grants DMR- 0820341 and DMS-1211087. This work was partially supported by Simons Foundation Grant 231015 (to S.T.).

1. Bernal JD (1965) *Liquids: Structure, Properties, Solid Interactions* (Elsevier, Amsterdam).
2. Zallen R (1983) *The Physics of Amorphous Solids* (Wiley, New York).
3. Manoharan VN, Elsesser MT, Pine DJ (2003) Dense packing and symmetry in small clusters of microspheres. *Science* 301(5632):483–487.

4. Gevertz JL, Torquato S (2008) A novel three-phase model of brain tissue microstructure. *PLOS Comput Biol* 4(8):e1000152.
5. Gillman A, Matouš K, Atkinson S (2013) Microstructure-statistics-property relations of anisotropic polydisperse particulate composites using tomography. *Phys Rev E Stat Nonlin Soft Matter Phys* 87(2):022208.
6. Quickenden TI, Tan GK (1974) Random packing in two dimensions and the structure of monolayers. *J Colloid Interface Sci* 48(3):382–393.
7. Ohring M (2001) *Materials Science of Thin Films* (Academic Press, San Diego, CA).
8. Azzam W, Cyganik P, Witte G, Buck M, Wöll Ch (2003) Pronounced odd-even changes in the molecular arrangement and packing density of biphenyl-based thiol SAMs: A combined STM and LEED study. *Langmuir* 19(20):8262–8270.
9. Cyganik P, Buck M, Azzam W, Wöll Ch (2004) Self-assembled monolayers of ω-biphenylalkanethiols on au(111): Influence of spacer chain on molecular packing. *J Phys Chem* 108(16):4989–4996.
10. Classen A-K, Anderson KI, Marois E, Eaton S (2005) Hexagonal packing of Drosophila wing epithelial cells by the planar cell polarity pathway. *Dev Cell* 9(6):805–817.
11. Farhadifar R, Röper J-C, Aigouy B, Eaton S, Jülicher F (2007) The influence of cell mechanics, cell-cell interactions, and proliferation on epithelial packing. *Curr Biol* 17(24):2095–2104.
12. Torquato S, Stillinger FH (2001) Multiplicity of generation, selection, and classification procedures for jammed hard-particle packings. *J Phys Chem B* 105(47):11849–11853.
13. O'Hern CS, Silbert LE, Liu AJ, Nagel SR (2003) Jamming at zero temperature and zero applied stress: The epitome of disorder. *Phys Rev E Stat Nonlin Soft Matter Phys* 68(1 Pt 1):011306.
14. Xu N, Blawzdziewicz J, O'Hern CS (2005) Random close packing revisited: Ways to pack frictionless disks. *Phys Rev E Stat Nonlin Soft Matter Phys* 71(6 Pt 1):061306.
15. Parisi G, Zamponi F (2010) Mean-field theory of hard sphere glasses and jamming. *Rev Mod Phys* 82:789–845.
16. Torquato S, Stillinger FH (2010) Jammed hard-particle packings: From Kepler to Bernal and beyond. *Rev Mod Phys* 82:2633–2672.
17. Charbonneau P, Corwin EI, Parisi G, Zamponi F (2012) Universal microstructure and mechanical stability of jammed packings. *Phys Rev Lett* 109(20):205501.
18. Dagois-Bohy S, Tighe BP, Simon J, Henkes S, van Hecke M (2012) Soft-sphere packings at finite pressure but unstable to shear. *Phys Rev Lett* 109(9):095703.
19. Torquato S, Stillinger FH (2007) Toward the jamming threshold of sphere packings: Tunneled crystals. *J Appl Phys* 102:093511.
20. Torquato S, Truskett TM, Debenedetti PG (2000) Is random close packing of spheres well defined? *Phys Rev Lett* 84(10):2064–2067.
21. Donev A, Torquato S, Stillinger FH, Connelly R (2004) Jamming in hard sphere and disk packings. *J Appl Phys* 95(3):989–999.
22. Krzakala F, Kurchan J (2007) Landscape analysis of constraint satisfaction problems. *Phys Rev E Stat Nonlin Soft Matter Phys* 76(2 Pt 1):021122.
23. Kamien RD, Liu AJ (2007) Why is random close packing reproducible? *Phys Rev Lett* 99(15):155501.
24. Scott GD, Kilgour DM (1969) The density of random close packing of spheres. *J Phys D Appl Phys* 2(6):863.
25. Berryman JG (1983) Random close packing of hard spheres and disks. *Phys Rev A* 27: 1053–1061.
26. Lubachevsky BD, Stillinger FH, Pinson EN (1991) Disks vs. spheres: Contrasting properties of random packings. *J Stat Phys* 64(3/4):501–524.
27. Atkinson S, Stillinger FH, Torquato S (2013) Detailed characterization of rattlers in exactly isostatic, strictly jammed sphere packings. *Phys Rev E Stat Nonlin Soft Matter Phys* 88(6):062208.
28. Kansal AR, Torquato S, Stillinger FH (2002) Diversity of order and densities in jammed hard-particle packings. *Phys Rev E Stat Nonlin Soft Matter Phys* 66(4 Pt 1):041109.
29. Jiao Y, Stillinger FH, Torquato S (2011) Nonuniversality of density and disorder in jammed sphere packings. *J Appl Phys* 109(1):013508.
30. Jullien R, Sadoc J-F, Mosseri R (1997) Packing at random in curved space and frustration: a numerical study. *J Phys I France* 7(12):1677–1692.
31. Torquato S (2002) *Random Heterogeneous Materials: Microstructure and Macroscopic Properties* (Springer, New York).
32. Lubachevsky BD, Stillinger FH (1990) Geometric properties of random disk packings. *J Stat Phys* 60(5/6):561–583.
33. O'Hern CS, Silbert LE, Liu AJ, Nagel SR (2004) Reply to comment on jamming at zero temperature and zero applied stress: The epitome of disorder. *Phys Rev E Stat Nonlin Soft Matter Phys* 70:043302.
34. Donev A, Torquato S, Stillinger FH, Connelly R (2004) Comment on "Jamming at zero temperature and zero applied stress: The epitome of disorder". *Phys Rev E Stat Nonlin Soft Matter Phys* 70(4 Pt 1):043301, discussion 043302.
35. Kausch HH, Fesko DG, Tschoegl NW (1971) The random packing of circles in a plane. *J Colloid Interface Sci* 37(3):603–611.
36. Shahinpoor M (1982) A model for crystallization of monomolecular layers on contracting surfaces. *J Colloid Interface Sci* 85(1):227–234.
37. Hinrichsen EL, Feder J, Jossang T (1990) Random packing of disks in two dimensions. *Phys Rev A* 41:4199–4209.
38. Frost R, Schön JC, Salamon P (1993) Simulation of random close packed discs and spheres. *Comput Mater Sci* 1(4):343–350.
39. Donev A, Torquato S, Stillinger FH, Connelly R (2004) A linear programming algorithm to test for jamming in hard-sphere packings. *J Comput Phys* 197(1):139–166.
40. Torquato S, Jiao Y (2010) Robust algorithm to generate a diverse class of dense disordered and ordered sphere packings via linear programming. *Phys Rev E Stat Nonlin Soft Matter Phys* 82(6 Pt 1):061302.
41. Donev A, Torquato S, Stillinger FH (2005) Pair correlation function characteristics of nearly jammed disordered and ordered hard-sphere packings. *Phys Rev E Stat Nonlin Soft Matter Phys* 71(1 Pt 1):011105.
42. Kansal AR, Truskett TM, Torquato S (2000) Nonequilibrium hard-disk packings with controlled orientational order. *J Chem Phys* 113(12):4844–4851.
43. Eden M (1961) A two-dimensional growth process. *Proceedings of the Fourth Berkeley Symposium on Mathematical Statistics and Probability*, ed Neyman F (Univ of California Press, Berkeley, CA).
44. Truskett TM, Torquato S, Debenedetti PG (2000) Towards a quantification of disorder in materials: Distinguishing equilibrium and glassy sphere packings. *Phys Rev E Stat Phys Plasmas Fluids Relat Interdiscip Topics* 62(1 Pt B):993–1001.
45. Skoge M, Donev A, Stillinger FH, Torquato S (2006) Packing hyperspheres in high-dimensional Euclidean spaces. *Phys Rev E Stat Nonlin Soft Matter Phys* 74(4 Pt 1): 041127.
46. Torquato S, Stillinger FH (2003) Local density fluctuations, hyperuniformity, and order metrics. *Phys Rev E Stat Nonlin Soft Matter Phys* 68(4 Pt 1):041113.
47. Donev A, Stillinger FH, Torquato S (2005) Unexpected density fluctuations in jammed disordered sphere packings. *Phys Rev Lett* 95(9):090604.
48. DeVries AL (1971) Glycoproteins as biological antifreeze agents in Antarctic fishes. *Science* 172(3988):1152–1155.
49. Knight CA, Duman JG (1986) Inhibition of recrystallization of ice by insect thermal hysteresis proteins: A possible cryoprotective role. *Cryobiology* 23(3):256–262.

Supporting Information: Existence of isostatic, maximally random jammed monodisperse hard-disk packings

Order Metrics

While we chose to focus on the order metric T^* in the main text, there are a number of other standard order metrics which have been used in the literature. Here, we will consider the bond-orientational order metric $\langle\psi_{6,k}\rangle$, defined as

$$\langle\psi_{6,k}\rangle = \frac{1}{N}\sum_{k=1}^{N}\frac{1}{N_{S,k}}\left|\sum_{j}^{N_{S,k}} e^{6i\theta_{k,j}}\right|, \tag{1}$$

where $N_{S,k}$ is the number of "bonds" that disk k has (equal to the number of edges on its corresponding Voronoi polygon), $\theta_{k,j}$ is the angle between some arbitrary reference direction and the vector connecting the center of disk j to the center of disk k, $i = \sqrt{-1}$, and $|\cdot|$ is the complex modulus [1]. The order metric $\langle\psi_{6,k}\rangle$ is positively-correlated with the translational order metric T^*; Figure S1 shows how these two order metrics compare via scatter plots of the (a) collectively and (b) strictly jammed packings from Figure 3 in the main text. For monodisperse packings, we prefer to use T^* because it is a non-local measure of order in the system in that it is not limited to information from near-neighbor disk pairs. This is important for monodisperse disks because because of their ability to exhibit locally-disordered areas that, on larger length scales, may not be disordered. A local measure such as $\langle\psi_{6,k}\rangle$ is susceptible to this subtlety. On the other hand, T^* is, by definition, an order metric that accounts for both local and non-local ordering. Because monodisperse packings have a tendency to exhibit long-range order, we prefer to use T^* instead of $\langle\psi_{6,k}\rangle$.

Comparison With Bidisperse Packings

In order to provide a comparison with two-dimensional disordered systems with which the average reader might be acquainted, we have computed the mean order map data for an ensemble of 1000 collectively and strictly jammed bidisperse disk packings (2000 in total) with diameter ratio $\alpha = 1/1.4$, number ratio $x = 0.5$ and system size $N = 400$ including ϕ and the order metrics T^* and $\langle\psi_{6,k}\rangle$. These data are compared to that of the ensemble averages and MRJ states for collectively and strictly jammed monodisperse spheres in Tables I and II. We find that the MRJ state of monodisperse disks more closely resembles the ensemble average of bidisperse disks for both collective and strict jamming–most so for strict

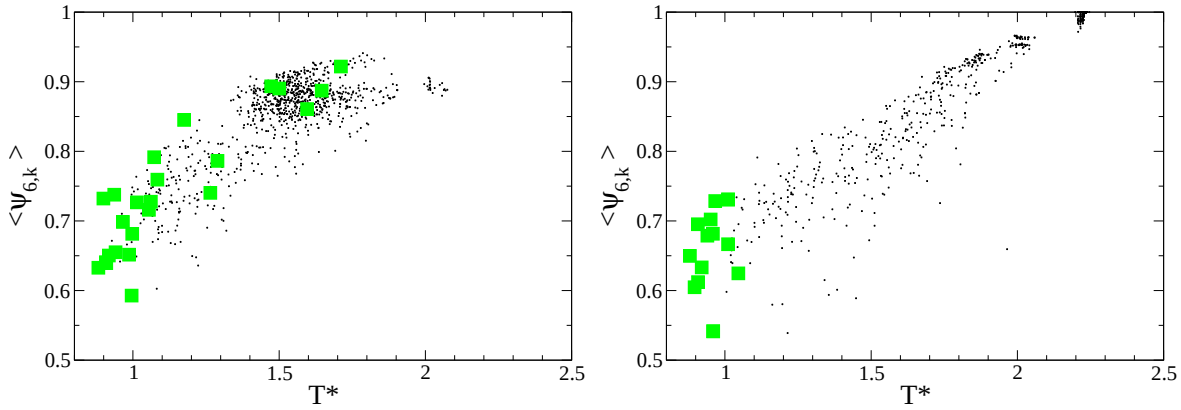


FIG. S1. (Color Online) Correlation of the order metrics T^* and $\langle\psi_{6,k}\rangle$ for (a) collectively jammed packings with $N = 150$ and (b) strictly jammed packings with $N = 110$ generated from RSA at $\phi_{init} = 0.10$. Isostatic packings are indicated as green squares.

TABLE I. Order map statistics for collectively jammed monodisperse and bidisperse disk packings

Packing	ϕ	T^*	$\langle\psi_{6,k}\rangle$
Monodisperse, ensemble average	$0.8612 \pm 1.2 \times 10^{-3}$	$1.55 \pm 1.8 \times 10^{-2}$	$0.859 \pm 6.0 \times 10^{-3}$
Monodisperse, MRJ state	$0.8268 \pm 1.2 \times 10^{-3}$	$1.01 \pm 1.9 \times 10^{-2}$	$0.676 \pm 1.0 \times 10^{-2}$
Bidisperse, ensemble average	$0.8384 \pm 1.5 \times 10^{-4}$	$0.871 \pm 8.8 \times 10^{-4}$	$0.538 \pm 9.0 \times 10^{-4}$

jamming and based on T^*. This is most likely because strict jamming allows the FC shape to become less of an issue and because T^* is more sensitive and long-ranged than $\langle\psi_{6,k}\rangle$.

In both cases (collective and strict jamming), the order of such binary disk packings changes continuously as the diameter ratio is brought to unity (wherein the monodisperse system is recovered); in addition, most packings generated are exactly isostatic when *any* degree of polydispersity is present. Interestingly, a size ratio of $\alpha = 1/1.01$ produces a distribution of packings in the order map plane that is very similar to that of the monodisperse case with the exception that isostatic packings are abundant instead of rare.

Note that it is nontrivial to extend the definition of T^* to a multicomponent system since it possesses multiple pair correlation functions. Here, we computed T^* as the simple mean of the four different pair correlation functions (i.e., for each pair combination of large and small disks).

TABLE II. Order map statistics for strictly jammed monodisperse and bidisperse disk packings

Packing	ϕ	T^*	$\langle\psi_{6,k}\rangle$
Monodisperse, ensemble average	$0.8784 \pm 1.6 \times 10^{-3}$	$1.94 \pm 2.2 \times 10^{-2}$	$0.921 \pm 6.5 \times 10^{-3}$
Monodisperse, MRJ state	$0.8255 \pm 2.3 \times 10^{-3}$	$1.00 \pm 4.7 \times 10^{-2}$	$0.663 \pm 2.4 \times 10^{-2}$
Bidisperse, ensemble average	$0.8391 \pm 8.9 \times 10^{-4}$	$0.873 \pm 8.4 \times 10^{-4}$	$0.540 \pm 3.0 \times 10^{-3}$

Ensemble Comparison with Lubachevsky-Stillinger Algorithm

How does the ensemble of packings created by TJ compare to that generated by other algorithms? Here, we compare an ensemble of 1000 packings created with TJ to an ensemble of 1000 collectively-jammed packings created with LS using an initial dimensionless densification rate of 10^2, which is known to produce configurations that are more disordered [2]. Both protocols used a system size of $N = 150$ and a square fundamental cell. Order maps for the TJ and LS ensembles are shown in Figures S2a and b, respectively. For the LS ensemble, the mean density was $\phi = 0.8780$ with a standard deviation of 1.40×10^{-2}; the mean order metric value was $T^* = 1.89$ with a standard deviation of 0.34. Figure S3 shows an example of the packings created by LS.

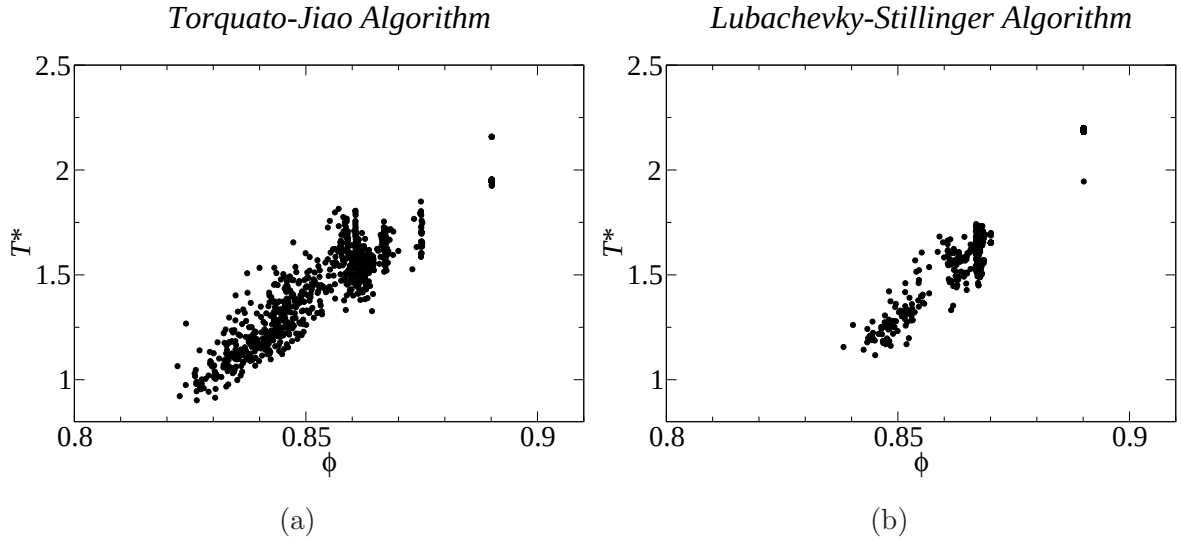


FIG. S2. Order maps of 1000 collectively jammed monodisperse disk packings made using the (a) TJ and (b) LS algorithms with a system size of $N = 150$ in a square fundamental cell.

Success Rate

Figure S4 shows the probability that an initial configuration, once compressed using TJ, will be

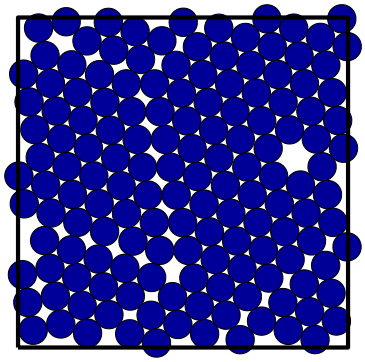


FIG. S3. (Color Online) An example of the polycrystalline packings generated by the Lubachevsky-Stillinger algorithm, $\phi = 0.8669$.

isostatic as a function of system size for some initial condition protocols and the constraint of collective jamming; error bars represent a 95% confidence interval using the Clopper-Pearson method [3]. The initial condition protocols shown are: RSA at a density of $\phi_{init} = 0.10$ with a square FC ("RSA, Square FC"), RSA at a density of $\phi_{init} = 0.10$ with a rhombic FC with interior angle $2\pi/5$ ("RSA, Distorted FC"), The Eden algorithm at a density of $\phi_{init} = 0.63$ ("Eden"), and the process detailed in the main text by which jammed bidisperse packings with size ratio $\alpha = 1/1.4$ and number ratio $x = 0.5$ were shrunk and re-jammed as monodisperse packings ("Bidisperse, $\alpha = 1/1.4$"). As the system size increases, it becomes progressively more difficult to obtain an isostatic jammed configuration as N increases; as an approximate rule of thumb, adding 40 disks to the system reduces the chances of finding an isostatic packing by approximately 10. Clearly, it is of interest to design a method of generating initial conditions that favor isostatic jammed states.

The probability of finding isostatic packings is lower when strict jamming is required. For most system sizes we tried, the success rate was on the order of 10^{-4}; 1 million or more packings might be needed per system size in order to infer success rates accurately enough to differentiate between system sizes.

Structure Factor

Figure S5 shows the structure factor for (a) collectively and (b) strictly jammed packings. These were computed using the same datasets used for the pair correlation function in Figures 7a and 7b of the main text: for collective jamming, the MRJ packings are 16 packings with $N = 150$ and 177 packings with $N = 100$ and the ensemble average is computed from 1000 randomly-selected packings made with TJ with $N = 150$; for strict jamming, the MRJ

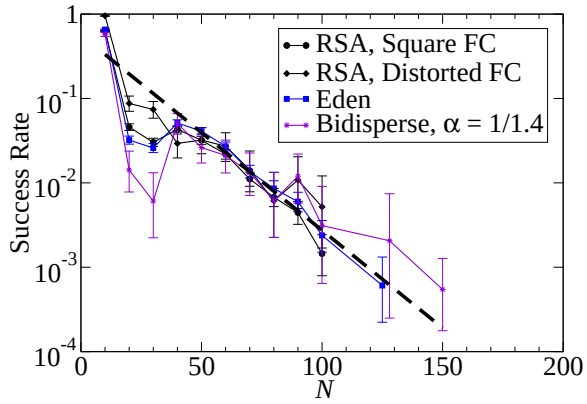
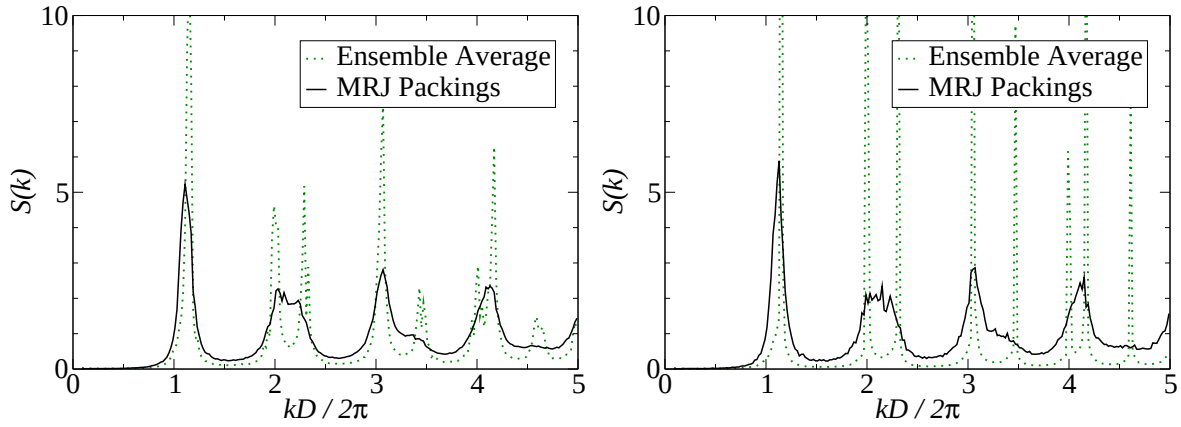


FIG. S4. (Color online) The probability that a packing of monodisperse disks will be exactly isostatic (i.e. the number of backbone contacts, Z, is equal to the isostatic number of backbone contacts, Z_{iso}) when jammed by TJ for collective jamming. In general, the probability decays at an exponential rate as the system size increases; a fit of the data gives $Pr(Z = Z_{iso}; N) = 10^{AN+B}$ where $A = -0.023$ and $B = -0.25$ (shown as a thick dashed line). Error bars correspond to a 95% confidence interval using the Clopper-Pearson method.

packings are 28 packings with $N = 110$ and the ensemble average is computed from 1000 randomly-selected packings made with TJ with $N = 110$. In a similar manner to the pair correlation function, we found that the spikes that are prominent in polycrystalline packings are considerably suppressed, indicating that the order that is characteristic of close packing in two dimensions has been significantly disrupted. The data is truncated at $k = 0.08$ because our systems are too small to resolve statistics for smaller wavenumbers.

Number Density Fluctuations

Our MRJ packings are not large enough to directly observe the long-wavelength behavior of the structure factor. However, we were able to determine that the MRJ state is hyperuniform by measuring the number density fluctuations. To do this, we repeatedly threw a circular window of radius R into our packings and counted the number of disk centers that fell within the window, $\langle N(R)\rangle$ as well as the the square of this quantity, $\langle N(R)^2\rangle$. If the number variance $\sigma(R) = \langle N(R)^2\rangle - \langle N(R)\rangle^2$ grows more slowly than the window area in two dimensions πR^2, then the system is hyperuniform[4]. Figure S6 shows $\sigma(R)$ for (a) collectively and (b) strictly jammed packings. Because this quantity grows more slowly than R^2, we conclude that the number density fluctuations are suppressed in the large-system limit. Data for the equilibrium fluid at $\phi = 0.60$ (for which $\sigma(R)$ scales as R^2) is shown for comparison.

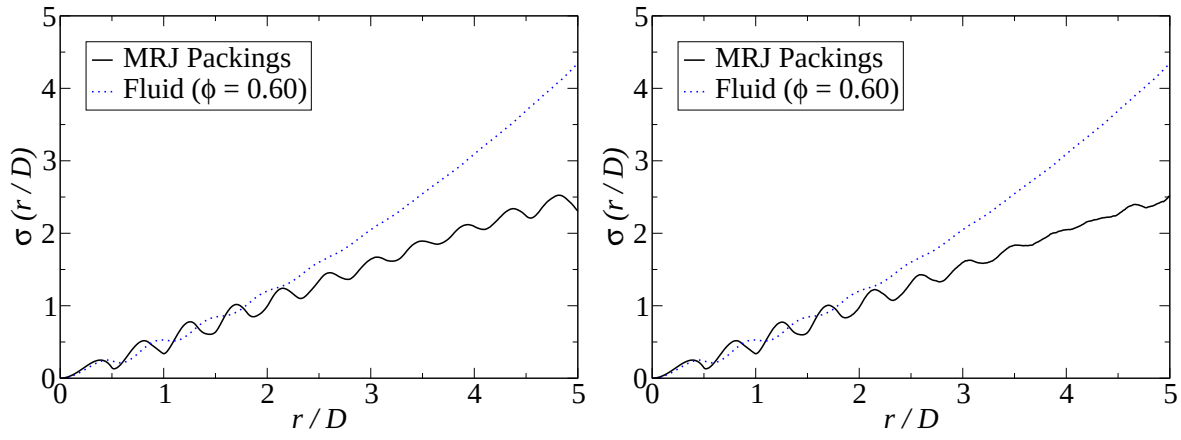


(a) (b)

FIG. S5. (Color Online) Structure factor for exactly isostatic, MRJ packings (black solid lines) and the ensemble average (dotted green lines) for (a) collective and (b) strict jamming, all generated using the TJ algorithm. As with the pair correlation function, harmonics that correspond to features of the triangular lattice that are readily found in polycrystalline packings are considerably suppressed in the MRJ state.

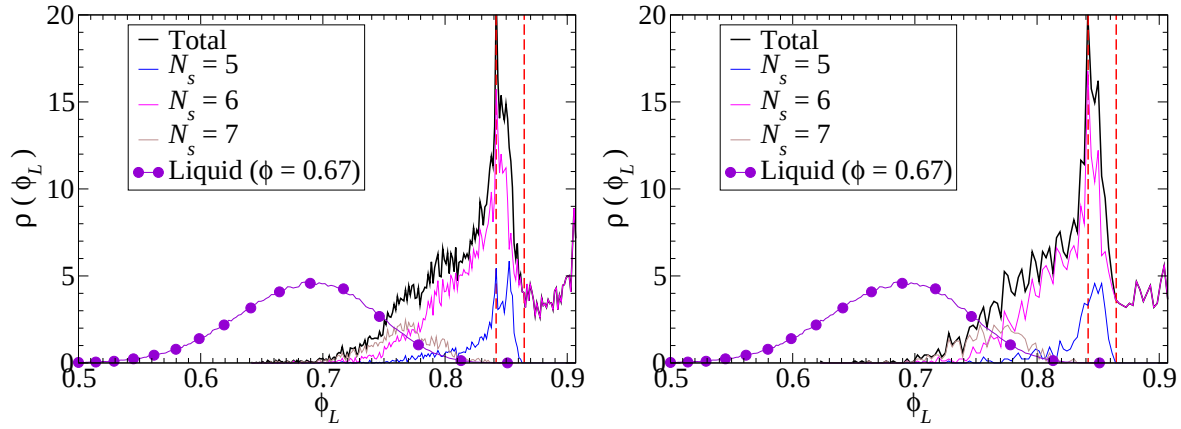
Local Packing Densities of the MRJ State's Voronoi Diagram

Figure S7 shows the MRJ packings' distribution of Voronoi cells' local packing fractions, ϕ_L, defined as the area of a single disk, v_1, divided the area of the Voronoi cell it occupies, v_c. The cell with the highest $\phi_L = \pi/\sqrt{12} = 0.9069\ldots$ corresponds to the hexagonal close-packed arrangement. The smallest Voronoi cell that we observed in our MRJ-like packings has a local packing fraction lower than this by 5.3460×10^{-7}. Since our packings are jammed to a contact tolerance of $10^{-9}D$, this deviation is caused by true near-contacts. Hexagons are the only type of Voronoi cell with $\phi_L \geq \pi/(5\tan(\pi/5))$. The smallest possible pentagonal Voronoi cell is the regular pentagon with local packing fraction $\phi_L = \pi/(5\tan(\pi/5) = 0.8648\ldots$ and the smallest possible heptagonal Voronoi cell has a local packing fraction just below $\phi_L = \pi/(2+\sqrt{3}) = 0.8418\ldots$, constructed by inserting two infinitesimally small edges into the pentagonal Voronoi cell shown in Figure S8.



(a) (b)

FIG. S6. (Color online) Number variance $\sigma(R)$ for (a) collectively and (b) strictly jammed packings. Because $\sigma(R)$ seems to grow more slowly for the MRJ packings than for the equilibrium fluid, number density fluctuations are suppressed in the large-wavelength limit, suggesting that the MRJ state is hyperuniform.



(a) (b)

FIG. S7. Probability density function for ϕ_L for (a) collectively and (b) strictly jammed MRJ packings. Dashed vertical lines are included that indicate the maximum ϕ_L for 5- and 7-sided Voronoi cells. The distributions are also decomposed according to number of sides in a cell. The distribution for the equilibrium liquid with $\phi = 0.67$ is shown for comparison.

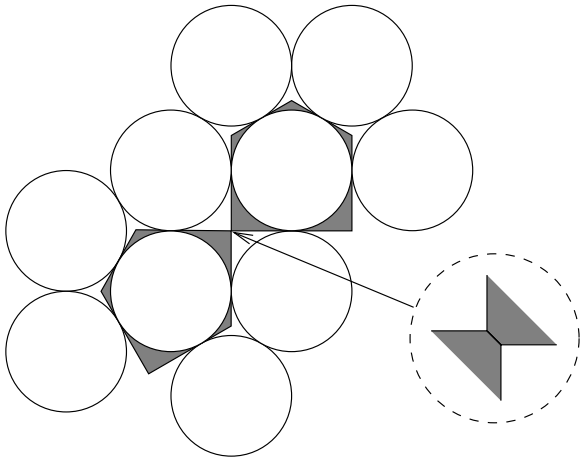


FIG. S8. Two common pentagonal Voronoi cells found in isostatic disk packings with local density $\phi_L = \pi/(2+\sqrt{3}) = 0.8418\ldots$. Small distortions in the disk packing can cause this Voronoi cell to gain an edge and become a hexagon, as shown in the zoom bubble, with a very small change in ϕ_L. Doing the same on the other similar corner creates the smallest heptagonal Voronoi cell.

[1] T. M. Truskett, S. Torquato, and P. G. Debenedetti. Towards a quantification of disorder in materials: Distinguishing equilibrium and glassy sphere packings. *Phys. Rev. E*, 62:993–1001, 2000.

[2] B. D. Lubachevsky, F. H. Stillinger, and E. N. Pinson. Disks vs. spheres: Contrasting properties of random packings. *J. Stat. Phys.*, 64(3-4):501–524, 1991.

[3] C. J. Clopper and E. S. Pearson. The use of confidence or fiducial limits illustrated in the case of the binomial. *Biometrika*, 26(4):404–413, 1934.

[4] S. Torquato and F. H. Stillinger. Local density fluctuations, hyperuniformity, and order metrics. *Phys. Rev. E*, 68:041113, 2003.